applied sciences

MDPI

Article

Discharge Electrode Degradation in Dry Electrostatic Precipitator Cleaning of Exhaust Gases from Industrial Solid Waste Incinerators

Tadeusz Czech [1], Artur Marchewicz [1], Arkadiusz Tomasz Sobczyk [1], Andrzej Krupa [1], Maria Gazda [2] and Anatol Jaworek [1,*]

[1] Institute of Fluid Flow Machinery, Polish Academy of Sciences, Fiszera 14, 80-231 Gdańsk, Poland; czech@imp.gda.pl (T.C.); amarchewicz@imp.gda.pl (A.M.); sobczyk@imp.gda.pl (A.T.S.); krupa@imp.gda.pl (A.K.)
[2] Faculty of Applied Physics and Mathematics, Gdansk University of Technology, Narutowicza 11/12, 80-233 Gdańsk, Poland; margazda@pg.edu.pl
* Correspondence: jaworek@imp.gda.pl

Abstract: The electrodes of industrial electrostatic precipitators degrade as a result of two phenomena: corrosion and erosion. The first is chemical degradation by highly reactive compounds formed during combustion, in particular, during the incineration of municipal or industrial wastes or high-sulfur coal. The degradation intensity of electrostatic precipitator electrodes depends on the chemical composition of the exhaust gasses. High concentrations of chlorides, fluorides, or sulfur in the exhaust gasses cause strong corrosion of the electrostatic precipitator elements. The second mechanism is the erosion caused by solid particles conveyed by the exhaust gas stream due to their collision with the electrodes. In this study, the analysis of the degradation of electrodes of an electrostatic precipitator downstream of an industrial waste incinerator was carried out. The industrial wastes of unknown sources were subjected to thermal degradation in a rotary kiln. The aim of this study was to provide fundamental knowledge about the mechanisms of electrode degradation located on the surface of discharge electrodes of electrostatic precipitators during the combustion of industrial wastes.

Keywords: electrostatic precipitator; electrode degradation; corrosion; fly ash; solid waste incineration

check for updates

Citation: Czech, T.; Marchewicz, A.; Sobczyk, A.T.; Krupa, A.; Gazda, M.; Jaworek, A. Discharge Electrode Degradation in Dry Electrostatic Precipitator Cleaning of Exhaust Gases from Industrial Solid Waste Incinerators. *Appl. Sci.* **2024**, *14*, 7616. https://doi.org/10.3390/app14177616

Academic Editor: Gerard Ghibaudo

Received: 11 July 2024
Revised: 8 August 2024
Accepted: 13 August 2024
Published: 28 August 2024

Copyright: © 2024 by the authors. Licensee MDPI, Basel, Switzerland. This article is an open access article distributed under the terms and conditions of the Creative Commons Attribution (CC BY) license (https://creativecommons.org/licenses/by/4.0/).

1. Introduction

The increasing amount of industrial solid waste produced by developed countries is a serious environmental problem. Hazardous wastes, including hydrocarbons, plastics, painted wood, paper, cartons, PET bottles, food remnants, and pesticides, are removed by their thermal degradation. Industrial solid waste is fed into a rotary kiln, where it is burned after minimal pre-treatment (only the largest non-flammable waste pieces are removed). A difference should be distinguished between municipal waste incineration plants, which operate practically continuously, and hazardous waste incineration plants, which operate discontinuously. In both types of waste incinerators, combustion products are usually very aggressive and lead to the degradation of exhaust-cleaning devices. When an electrostatic precipitator is used to remove particles from exhaust gasses, the corrosion and/or erosion of the electrodes is a significant problem. These processes result in rapid loss of electrode material, thereby reducing the collection efficiency of this type of device.

The problem of corrosion–erosion processes occurs in many devices in which a working medium, gas, or liquid conveying small solid particles flows at a high velocity. Devices operating in the process of thermal degradation of industrial waste are particularly exposed to corrosion and erosion. In the case of thermal power plants, the problem of erosion–corrosion occurs in electrostatic precipitators (ESPs), in which the flue gas contains dust particles. The erosion damage of metal structures caused by an impact of solid particles has

been discussed, for example, by Malcher [1]. In the case of electrostatic precipitators, the consequence of the erosion process is the serious degradation of electrodes and insulators, which results in a decrease in the collection efficiency [2] and the premature failure of structural parts, causing the generation of additional costs associated with the need for their replacement.

The production of industrial solid waste has increased significantly over the past 60 years. In 1960, approximately 88 million tons of industrial waste was produced in the United States, and by 2018, this figure increased more than three times, to 292 million tons [3]. In particular, due to population growth and urbanization in developing countries, the generation of municipal and industrial solid wastes has also increased significantly over the past decades and is expected to be doubled by 2025 compared to 2012 [3]. The incineration of industrial solid waste is widely used to solve the problem of the large volume of waste that modern society produces [4]. The thermal treatment of wastes is the most frequently used method of waste disposal, but these processes are not fully acceptable under current international environmental policy, which prefers the efficient recovery of raw materials and energy. Incineration plants have many advantages over other waste-disposal methods, such as reduced volume and weight after the incineration of waste and the biological detoxification of ash. However, the flue gas contains high concentrations of polycyclic aromatic hydrocarbons (PAHs) [5] and fly ash with heavy metals [6]. The thermal decomposition of industrial wastes requires cleaning the exhaust gasses of toxic products, which are released into the atmosphere and can influence human health [7,8].

Fly ash also contains a large number of compounds, including carbon as soot particles, dioxins, furans [9], and compounds of toxic metals: arsenic, cadmium [10], chromium, nickel, and mercury bichloride [11]. Within the techniques of cleaning gasses from industrial waste incinerators, electrostatic precipitators and fabric filters meet the exhaust gas-treatment standards [12].

In the process of waste incineration, not only solid particles but also noxious and corrosive gasses are produced. In the process of waste combustion, most of the sulfur contained in the fuel is transferred (in an oxidizing atmosphere) to sulfur oxides [13]. Sulfur dioxide already in the furnace turns into sulfur trioxide. Also, during an electric discharge in an electrostatic precipitator, compounds such as nitrogen or sulfur oxides (NO_x and SO_x) are produced due to the presence of fast electrons, forming free radicals in collisions with gaseous molecules. The harmfulness of SO_3 lies in the fact that it condenses on the surface of the devices after reaction with water in the form of sulfuric acid, which creates strong metal corrosion. Due to the low velocity of solid particles in the exhaust gas stream (about 1 m/s) and their low kinetic energy, the erosion process is less important, although a long time of impact of solid particles of different morphologies onto the discharge electrodes of electrostatic precipitator can also locally erode or deform its surface, which leads to electrode failure and electrostatic precipitator accidents.

In practice, after such an accident, due to the lack of knowledge of the chemical composition of flue gasses and properties of conveyed fly ash particles, which were precipitated earlier, it is not easy to distinguish between these two processes during actual electrostatic precipitator operation. Only the results of the degradation can be assessed by experts after years of ESP operation.

The problem of electrode material degradation in electrostatic precipitators has not been sufficiently thoroughly studied in the literature. There are only a few papers on this subject referring to dry ESPs, particularly those operating in harsh conditions of waste incinerators. The degradation of electrodes in the electrostatic precipitator reduces the performance of the electrostatic precipitator, mainly its collection efficiency, which results in increased particulate matter emission released into the atmosphere. The production of electrodes from the high-corrosion- and erosion-resistant materials can increase the lifetime of these electrodes and reduce the costs of electrodes replacement but increases the investment costs. Three types of solutions can be met in scientific and engineering papers, which are used to increase the lifetime of discharge electrodes: (1) the coating

of the discharge electrode with an acid-resistant layer, (2) using the composite discharge electrodes, and (3) the construction of two-stage electrostatic precipitators, with the charging stage equipped with an ion injector instead of a conventional discharge electrode.

The electrodes with acid-resistant coating were constructed and investigated by Machnik and Nocuń [14]. The authors used a mast electrode with blade emission elements, and a cylindrical smooth rod electrode, both with and without an anti-corrosion coating. Tests were conducted by the authors in order to assess the performances of three anti-corrosion agents: (1) "Unikor C" with an iron (III) oxide filler, (2) a water-soluble acrylic resin polydispersion, with an organic filler, and (3) a polyurethane varnish without a filler. The thickness of these coatings was between 50 and 65 µm. The measurements were carried out in the ambient air, at a pressure of 987.9 hPa, a temperature of 22 °C, and relative humidity of 53%. The authors measured the discharge current, the corona onset voltage, and the current density distribution on the collection electrode, for all the discharge electrodes tested. Their findings indicated that the anti-corrosion coating does not significantly affect these electrodes' parameters. The addition of Fe_2O_3 (15 wt.%) to the coating resulted in an increase in the discharge current of the electrodes with blades.

Ali et al. [15] developed a novel hybrid composite discharge electrode made of carbon fiber composite combined with metal mesh, which exhibited corrosion resistance and lightweight properties. This type of electrode could potentially be used in a wet electrostatic precipitator as a superior alternative to traditional metal electrodes. The hybrid composite discharge electrode exhibited a lower corona onset voltage than conventional metal electrodes, and the corona discharge was more uniform at comparable power levels.

A two-stage electrostatic precipitator, designed for the removal of particles and acidic droplets (for example, HF, HCl, HNO_3, and H_2SO_4) from corrosive gasses, discharged from the wet-etching technologies in semiconductor and optoelectronic industries, and from explosive gasses, as developed by Kim et al. [16]. The precharger stage consisted of ion injectors with clean air sheath, placed outside the main gas flow, and constructed from carbon brush. The carbon electrodes were more resistant to the corrosive atmosphere than those made of metal. The collection efficiency for PM2.5 particles, achieved by this device, was between 89.5% and 99.5%, depending on the brush electrode depth, by a voltage applied to the carbon brush emission electrodes of −23 kV, and the exhaust gas flow rate of 600 L/min.

Hall and Katz [17] considered the problem of mechanisms of the corrosion of electrodes in electrostatic precipitators. The authors identified the following types of corrosion specific to electrostatic precipitators, from which the most important are the following:

Uniform attack—this appears in the case the electrode has a direct contact with acids, caustics, or other corrosive liquids separated from the gas on a large surface of the electrode. The most susceptible to these attacks are collection plates, gas distribution baffles, hoppers, shells, roof, and isolator supports, and particularly the surfaces, which are locally cooled due to imperfect thermal isolation.

Pitting—this is an intense deep corrosion in small areas (points), particularly in the breakdowns of protective coating. The most vulnerable to this type of corrosion are discharge electrodes and rappers, and places through which cold air is drawn in.

Stress corrosion—this occurs in places loaded with high tensile stress in the presence of corrosive atmosphere. The discharge electrode frames are susceptible at their bents to this type of corrosion due to microcells formed in the material in the fabrication process.

Crevices corrosion—this is a type of corrosion occurring in tight gaps between two different parts in contact, for example, under gaskets, seals, washers, and screws, or inside cracks and seams. This type of corrosion may occur in all connections of different parts in an electrostatic precipitator.

Intergranular corrosion—this appears along material grain boundaries, particularly those formed due to material stress during cooling after welding. This type of corrosion may occur in the shells and roof, as well as in collection or discharge electrodes.

Fatigue corrosion—this results from a cyclic load or stress in a corrosive atmosphere. This fatigue leads to the formation of micro or macro cracks. The rappers, rapper anvils, particularly in welded areas, or hangers of collection plates are loaded by excessive vibration during rapping or the discharge electrodes.

Impingement attack—in the case of electrostatic precipitators, this is a process of scouring the metal surfaces exposed to the flowing abrasive media, leading to its erosion or surface attack through the scale, which are the corrosive products.

Fretting corrosion—this is the high frequency vibration of the collection and discharge electrodes during their rapping, which leads to metal fit erosion as an effect of friction.

Galvanic action—this corrosion occurs in a junction between two metals of different electrochemical potentials in the galvanic series. This localized metal erosion occurs particularly in the connections of discharge electrodes to a high voltage source.

In many practical cases all the mentioned mechanisms operate simultaneously, providing a synergistic effect in the electrode's failure, and the final electrode degradation reasons are difficult to distinguish. Regarding the collection electrodes, the most susceptible to corrosion are plates adjacent to the chamber outer walls or hoppers, where the gas temperature can drop below the dew point for acid condensation [17]. The upper parts of the collection and discharge electrodes can be exposed to the infiltration of cold air through the supporting insulators. Electrodes can also be eroded by excessive electrical breakdowns or electrical coronas due to the misalignment of the electrodes, sharp edges remaining after their fabrication, or thermal bending [17].

The erosion of metal surfaces caused by bombardment by a stream of solid particles conveyed by the flowing gas was investigated numerically by Malcher [1]. The collision of such particles with the metal surface can remove microscopic fragments of material from the surface. In the case of electrostatic precipitators, the most heavily loaded areas are the duct sidewalls, vanes, and baffles, where the gas velocity is of several m/s. The author assumed that a solid particle approaches the metal surface at an impingement angle, γ (the angle between the surface and incident trajectory), with velocity V_p. It was also assumed that the particle is much harder than the metal surface, the particle does not break up after collision, and the metal surface deforms plastically. The model of erosion was based on that provided by Finnie [18], which is valid for ductile materials:

$$E = kV_p^n f(\gamma) \quad (1)$$

where E is the volume of material removed by a single abrasive particle, k is a constant depending on the hardness of eroding metal and the mass of the particle, V_p is the velocity of the impinging particle, n is the coefficient determined experimentally, γ is the impingement angle, and f is the dimensionless wear function, depending on the impingement angle γ.

The objective of this article was to investigate the mechanisms of discharge electrode degradation in an industrial electrostatic precipitator operating downstream of an industrial waste incinerator. The analysis discusses the most plausible mechanisms leading to the observed degradation results. These mechanisms have been reconstructed ex-post, because the operating conditions of the incinerator, the chemical composition of exhaust gasses, and the PM content are not known and can largely vary in real exploitation conditions. To this end, the traces of elements remaining in the electrode material were analyzed as potential markers of the corrosion process.

The main goal of this article was to address the main mechanisms of the discharge electrodes' degradation in an electrostatic precipitator operating under harsh conditions of an industrial waste incinerator, which are significantly different from those characteristic of coal-fired power plant boilers.

This paper presents novel insights into the potential mechanisms of electrode degradation under real-world, harsh operational conditions. The provided information will assist in selecting appropriate electrode material and/or implementing protection against the action of various factors, in order to extend the maintenance period.

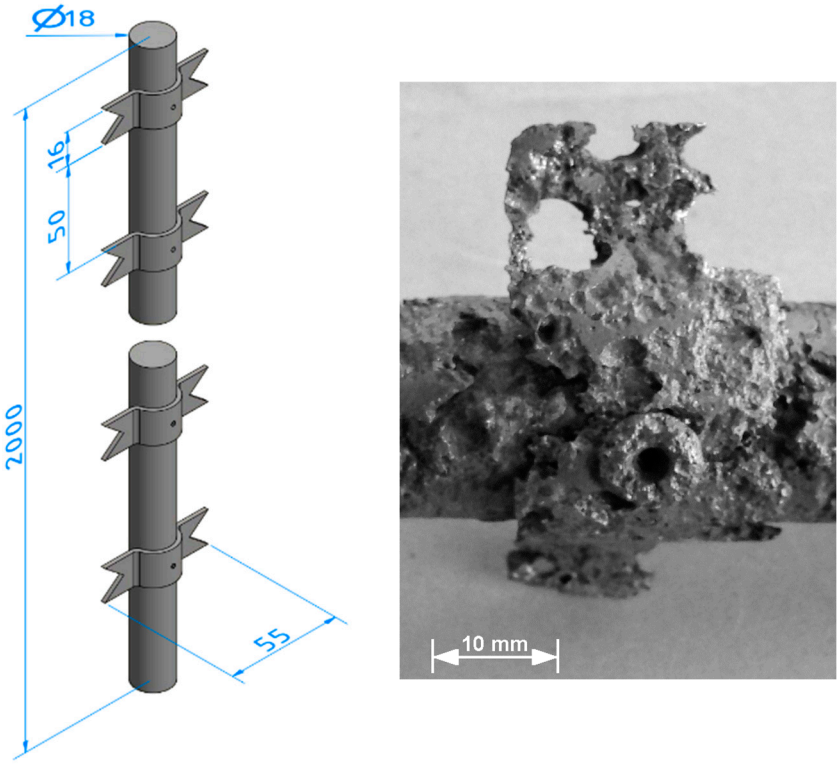
2. Materials and Methods

2.1. Subject of Study

This paper presents the analysis of the mechanisms of the degradation of a discharge electrode of an electrostatic precipitator used for cleaning flue gasses produced by a solid waste incinerator, composed of a rotary kiln, in which various undefined industrial wastes are combusted.

The effects of the degradation processes on a corona discharge electrode, after a period of more than two years of operation in a dry electrostatic precipitator, were analyzed using Scanning Electron Microscopy (SEM), Energy Dispersive Spectroscopy (EDS), and X-ray Diffraction (RDX) methods. The ESP was used for the removal of particles from exhaust gasses generated during the combustion of industrial wastes of an unspecified composition in a rotary kiln operating at a temperature of about 1100 °C. The cylindrical electrostatic precipitator was equipped with the discharge electrodes in the form of an array of spiked blades riveted to the cylindrical pipe. The electrodes were powered by a voltage of about 60 kV of negative polarity.

A drawing of the discharge electrode design is shown in Figure 1a. An example of a degraded discharge electrode, after about two years of operation, is shown in Figure 1b. Two close-up views of the degraded fragments of these blades are shown in Figures 2 and 3. Figure 1b shows a damaged element of the discharge electrode covered with corrosion products and dust. The issue of electrode degradation is of significant concern, because it entails the costly replacement of the damaged electrodes with new ones, which generates financial costs for the incinerator factory.



(**a**) (**b**)

Figure 1. Sketches of the discharge electrode of an electrostatic precipitator (**a**), and a single pair of discharge blades degraded as a result of the action of dust, acid gasses, and electric discharges (**b**). Electrode material: austenitic chromium–nickel steel (cf. Table 1).

Table 1. Elemental compositions (in wt.%) of selected spots on the surface of the discharge electrode of an electrostatic precipitator.

Sampling Location	Carbon	Oxygen	Silicon	Sulfur	Chromium	Iron	Nickel
Inlet dust	44.70	20.21	0.47	5.79	4.81	1.60	0.01
Original electrode material	0.39	≤0.01	0.67	≤0.01	17.46	66.72	10.50
Degraded electrode surface	66.72	20.90	0.32	3.33	1.48	3.37	≤0.01
Scale on the electrode	8.59	45.87	0.41	2.55	5.43	12.14	0.94



Figure 2. A fragment of a sharp electrode with its tip deformed probably as a result of DC back-corona discharge. (Photo taken with Optical Digital Microscope Keyence VHX7000N, courtesy of the company Keyence (Osaka, Japan)).

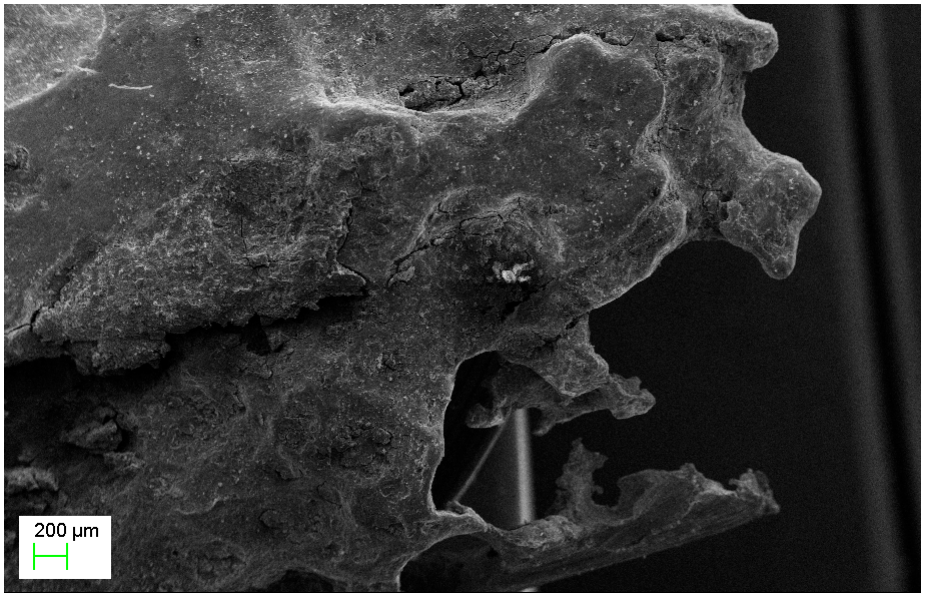


Figure 3. SEM micrograph of thermally deformed tip of blade electrode of electrostatic precipitator.

The discharge electrodes of the electrostatic precipitator under consideration were in the form of pipes with a diameter of 18 mm and attached spiked blades (schematically

shown in Figure 1a). During the operation, the sharp tips of the blade electrode were degraded due to acid gas attacks and high temperature generated by pulseless corona discharge (Figure 1b).

2.2. Experimental Methods

The morphology of degraded discharge electrode surface and dust deposited on the discharge electrode was studied under a scanning electron microscope EVO 40, Carl Zeiss, Oberkochen, Germany. The elemental compositions of the dust particles and the electrode were analyzed using EDS (Quantax 400, Bruker Corporation, Billerica, MA, USA). The qualitative and quantitative chemical analysis of the atomic composition of the discharge electrode material was obtained. The analyzer was equipped with a detector XFlash 5010 SDD for the detection of elements ranging from boron (0.185 eV) to americium (1.8 keV), with a maximum energy resolution of 125 eV for the Mn Kα line.

The mineralogical composition of the degraded material of the discharge electrode was detected with an X-ray diffractometer system X'pert, PRO-MDP Philips (PANalytical, Almelo, The Netherlands) with cooper K_α radiation (λ = 1.5404X) in the scattering range of 20–80°. The constituent crystal phases of the particles were identified using the High Score Plus software (version 3.Oe (2012)) operating with the diffractometer.

Some images were taken using Optical Digital Microscope Keyence VHX7000N (Keyence Corporation, Osaka, Japan) with FI Head (VHX-7100 + E500 lenses). This digital microscope was capable of capturing high-resolution images and measurement data. A profile of the surface of the discharge electrode tip was obtained with 3D Optical Profilometer Keyence VR-6200 (Keyence Corporation, Osaka, Japan).

3. Results

To identify the potential causes of the discharge electrode degradation, various areas of the electrode were analyzed: the areas of the cracked surface, the deposits on the edges of open pits, and the cross-sections of the cylindrical element of the electrode.

3.1. Thermal Electrode Deformation

An optical photograph of a tip of a molten blade electrode of an electrostatic precipitator is shown in Figure 2, and a SEM micrograph of thermally deformed material, in Figure 3. These deformations may be a result of back corona or other electric discharges between the electrodes. Back-corona discharge streamers between the discharge electrode and the collection electrode covered with a resistive layer (fly ash) develops into back-corona glow, which forms a local (spot) at the discharge electrode tip [19,20]. Pulseless glow back-corona discharge in a flue gas is characterized by a high current density and a small voltage drop between the cathode and the anode. The cathode temperature during this discharge can be very high (>1000 °C), and the plasma column forms a narrow, brightly glowing channel between the electrodes. The electrical discharge that could arise generates significant amounts of heat in the area of the electrode tip [21,22]. The melting of the electrode surface and evaporation of the electrode material were a result of the increased temperature at this point [23,24], followed by a local formation of characteristic round shapes and/or the droplets of molten material (bound by cohesive forces; Figure 2). An additional effect of this process, while prolonging, may be a thermal deformation of the electrode blades (Figure 3). The hypothesis on the thermal deformation is supported by the fact that the amount of corrosive agent (sulfur) is insignificant in the material of the tip of deformed electrode blade (cf. Table 1).

In Figure 2, the edge of the blade electrode affected by the back-corona discharge changes its shape, and a melted area can be seen as a droplet on the edge of the electrode blade. As a result of the pulseless back-corona discharge, at the point of its initiation, a fragment of material melts and vaporizes under the influence of high temperature in the plasma column. The molten metal, under the influence of cohesive forces, forms characteristic round shapes or droplets. The degree of melting of the material depends

on the material used, the discharge current density, and the exposure time. The nickel–chromium alloys used as the electrode material (cf. Section 3.3) have high corrosion resistance in the temperature range up to 200 °C, making these alloys suitable for many applications (including electrical discharge plasma).

3.2. Size and Elemental Composition of Fly Ash Particles Precipitated in ESP

The properties of fly ash particles collected from the discharge electrode of the investigated electrostatic precipitator, after the incineration of industrial wastes of mixed composition in the rotary kiln, were investigated using SEM micrographs and EDS analysis. SEM micrographs of solid particles removed from a discharge electrode are shown in Figure 4a,b. The shapes of these particles are not regular, different from the particles from burning bituminous coal [25], which are mostly spherical.

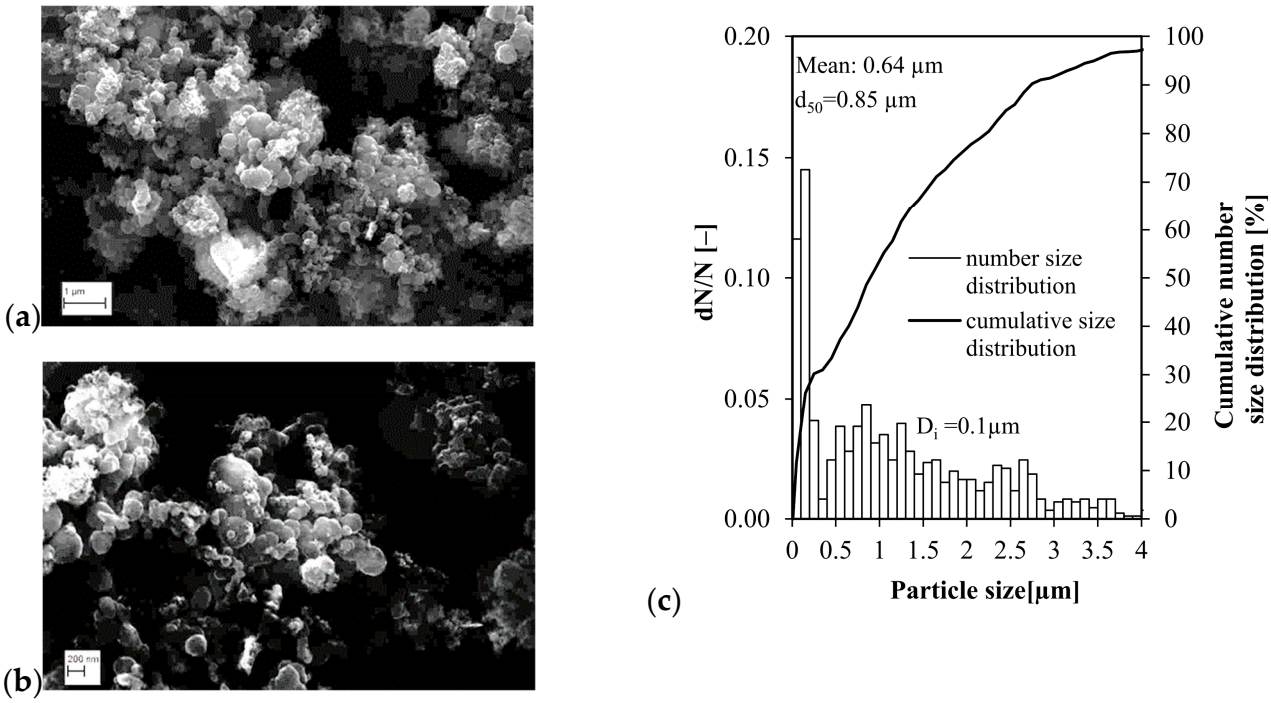


Figure 4. SEM images of fly ash particles collected from discharge electrode: magnification ×25,000 (**a**) and magnification ×50,000 (**b**), and number and cumulative size distribution of fly ash particles (**c**). Resolution of particles size: 0.1 µm.

The number and cumulative size distribution of fly ash particles determined from the SEM micrographs are shown in Figure 4c. The size of the particles ranged from about 400 nm to 10 µm or larger. The mean value of the size of the fly ash particles was 0.64 ± 0.012 µm, and the median was equal to 0.51 µm (Figure 4c). The finest particles are formed due to the condensation of vapors of vaporized mineral substances contained in the industrial wastes. The EDS spectrum showing the elemental analysis of fly ash from the combustion of industrial waste is shown in Figure 5.

To avoid corrosion, the process of particle precipitation should be carried out in such a way as to maintain the temperature above the acid dew point in the entire space of the electrostatic precipitator.

The fly ash from the industrial waste incinerator consists mainly of silicon, aluminum, calcium, potassium, and copper. The dust contains a high percentage of unburned carbon (probably in the form of hydrocarbon chains). The sulfur content is 6.21%, that of chlorine is 0.25%, and the sum of alkaline elements (sodium, magnesium, calcium) is approximately <2%. These data also contain small amounts of chromium, nickel, and iron, which

could be components of the discharge electrode. Large particles are formed through the agglomeration of smaller primary particles in or outside the burning chamber.

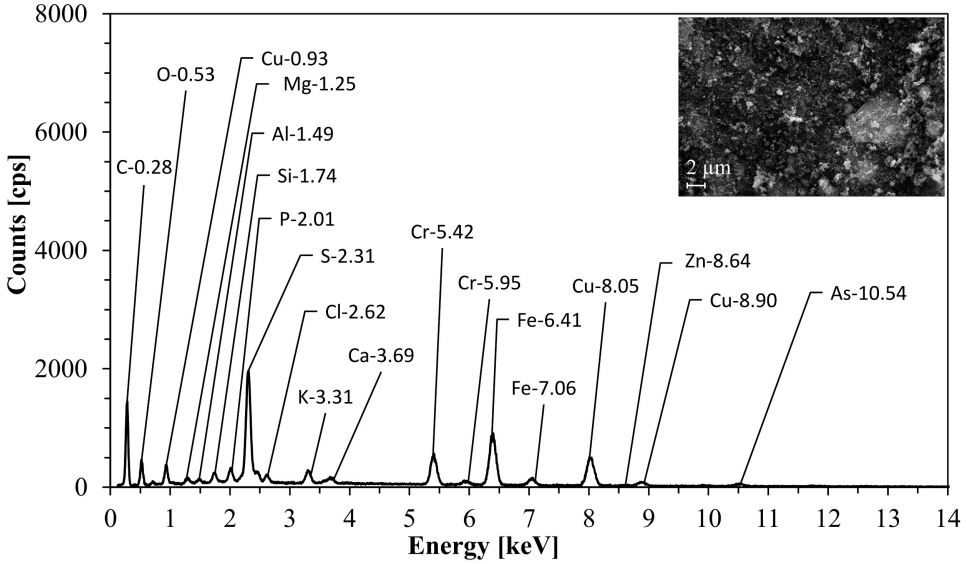


Figure 5. EDS spectrum of fly ash collected from discharge electrode in electrostatic precipitator after combustion of industrial solid waste. Inset: investigated sample of ash.

3.3. Analysis of Elemental Composition of Discharge Electrode Material

The external surface of the corroded discharge electrode and a clean cut of the electrode were analyzed using the EDS method. Some specimens, approximately 5 mm thick and 18 mm in diameter, were cut from the pipe supporting the spiked blades of the discharge electrode, perpendicularly to its axis (cf. Figure 1a) in order to analyze the chemical composition of the original electrode material. The EDS spectrum showing the elemental analysis of the material of the discharge electrode in various places is shown in Figure 6.

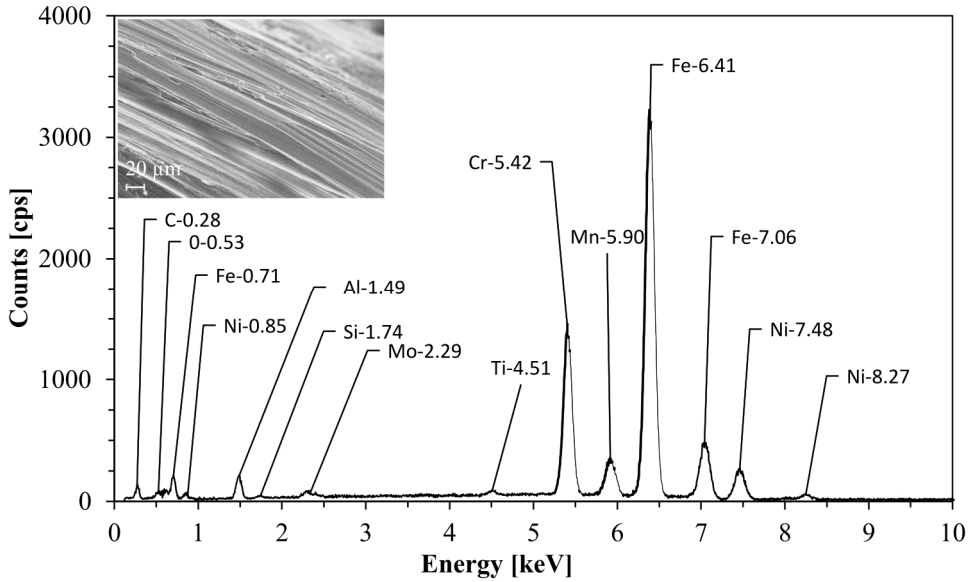


Figure 6. EDS spectrum of clean surface of discharge electrode material after cutting (inset: image of cross-section of test sample).

The electrode material was cleaned and analyzed in selected, non-corroded places. The elemental composition of the discharge electrode in various places is presented in Table 1.

The results obtained for the cut surfaces indicate that the discharge electrode was made of austenitic chromium–nickel steel, probably type 316 Ti, with the following composition: Fe (≤73%); Si (≤1%); S (≤0.01%); P (≤0.015%); Ni (≤20.5 ÷ 13.5%); Mo (≤3%); Mn (≤2%); Cr (≤16.5 ÷ 18.5%) Al (≤1.0%); and C (≤0.05%) (cf. Figure 6). This type of steel is generally used for the construction of electrodes of electrostatic precipitators due to its high hardness, flexibility, and modulus of elasticity.

This composition of the electrode material can be changed at its surface due to chemical interaction with exhaust gasses (NO_x, SO_x) and the radicals produced in the electric discharge generated by a high voltage applied to the discharge electrode, and interaction with fly ash particles. The changes in the elemental composition of these characteristic places will be discussed in the following sections.

3.4. Changes in the Surface of Discharge Electrode Materials after Operation

Stress corrosion cracking occurs when the electrochemical reactions occur together with mechanical stress. The corrosion of this type, acting with dislocations in the metal crystal structure, may manifest itself as intergranular or intragranular cracking.

The issues of durability of materials in gasses produced during waste combustion are extremely important in the design and construction of gas cleaning installations. The construction failure is mainly caused by the material loss due to corrosion and/or erosion. Due to the low velocity of fly ash particles in the electrostatic precipitator (about 1 m/s), and their relatively small mass, the kinetic energy of ash particles is too low to cause significant erosive changes in the discharge electrodes; however, local stresses in the electrode material may occur, deforming its surface. In addition, the impinging particles may remove fragments of corroded material increasing the exposure of electrode to further corrosion, which can result in a synergistic corrosion–erosion effect. In Figure 7, the occurrence of the plastic deformation of the surface in the form of the waving of the metal surface (probably caused by the existence of mechanical forces), and spherical cavities, which can be the pits remaining after back-corona discharge, can be noticed. Abrasion is a purely mechanical effect, and abrasive wear occurs when a metal element is abraded by dry mineral particles of much greater hardness. Abrasive wear is visible in the form of grooves and peelings of the surface (Figure 7).

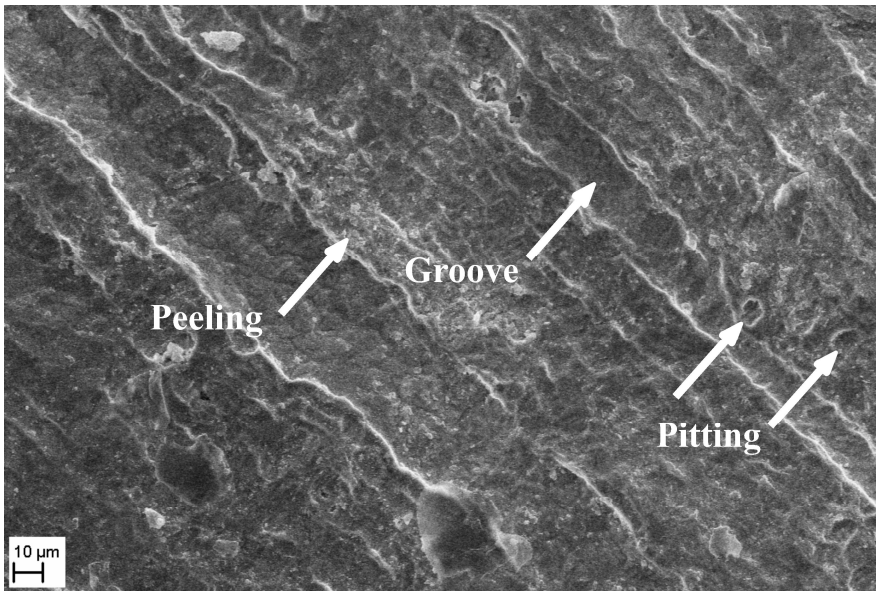


Figure 7. SEM image of microdeformation of discharge electrode blade.

General corrosion (uniform attack; Hall and Katz [17]) is characterized by a uniform loss of the surface layer as a result of the reaction of aggressive components of the gaseous environment with the construction material, usually metal. Many metals and structures

are subject to corrosion damage due to the aggressiveness of the environment and the simultaneous action of mechanical factors, like erosion or stress. In many devices in which solid particles flow with a high velocity (of high kinetic energy)—for example, in dust-conveying ducts—the erosion process also occurs. In a gas produced by waste incineration, these two processes complement each other, destroying the structure of the material. In the case of devices operating at a high voltage, the material surface can also be subjected to electric discharges, which can lead to local material melt and/or evaporation.

Pitting corrosion is a type of local corrosion that occurs in a limited area, and a significant part of the surface is not attacked [17]. In the analyzed surface, the pitting corrosion appears in the shape of hemi-spherical pits, the depth of which, in many cases, is greater than their diameter (cf. Figure 7).

3.5. Cracks in the Electrode Material

Fatigue changes are related to the formation of fatigue cracks as a result of mechanical plastic or elastic deformation in a corrosive environment and are shown in Figure 8. The cracks in material structure allow the acid gasses (SO_2 or HCl) to penetrate deeper into the layer, facilitating further corrosion. The degradation processes caused by the electrode corrosion are of great importance, both for the mechanical strength of the device structure and for the efficiency of the electrostatic precipitator, especially because the changes in the shape of the electrode (the electrode deformation and sharpness of the emission points) can reduce the discharge current and/or electric field.

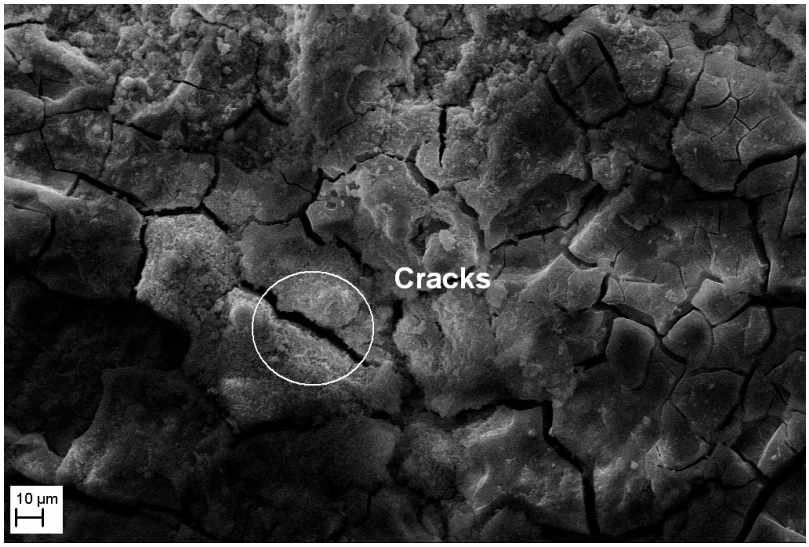


Figure 8. SEM of electrode surface showing the initial process of corrosion as cracks. A crack is marked with a white circle.

As the relative humidity increases, HCl or H_2SO_4 nuclei are formed, which can react with the electrode material, creating the pits in it, as shown in Figure 7. The electrode degradation, from shallow pits to canyon-like structures, and corrugated surfaces, are surrounded by metal oxides, but sometimes also by chlorides or sulfates [26]. It should be emphasized that the chloride seams regularly appear directly at the site of corrosion.

The acidic (SO_2 or HCl) components of the exhaust gasses penetrate through the cracks in the metal surface. In assuming the complete dissociation of H_2SO_4 into H^+ and SO_2, for the acid corrosion of any metal, Me, regardless of the type of acid, the following reactions can occur [26]:

$$(\mathrm{Me})_{stable} + (\mathrm{H_2SO_4})_{liquid} \longrightarrow (\mathrm{MeSO_4})_{stable} + (\mathrm{H_2})_{gas}$$

or for oxysulfides,

$$3\mathrm{Me} + \mathrm{SO_2} \longrightarrow \mathrm{Me(S,O)} + \mathrm{MeS}$$

The EDS analysis presented in Figure 9 confirms the validity of these reactions, because some sulfur compounds are present within the cracks and on the metal surface (see Figures 5 and 9).

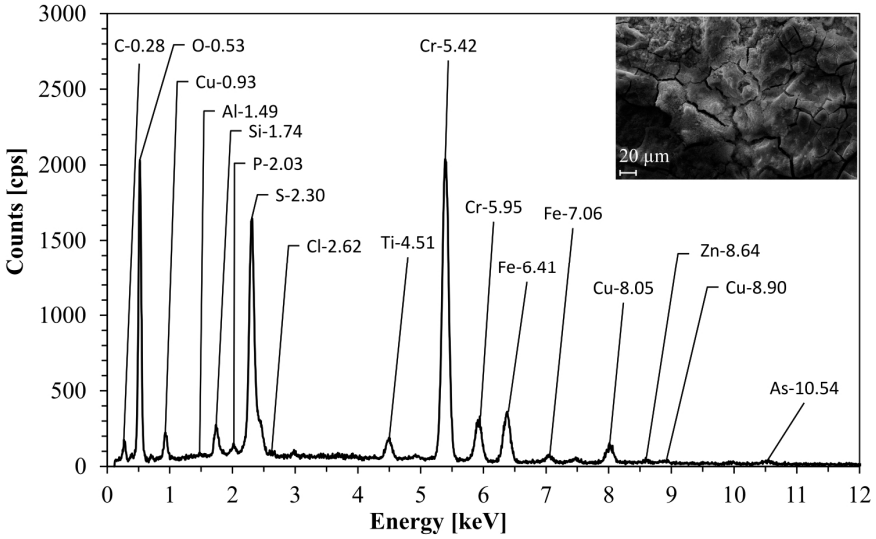


Figure 9. EDS spectrum of cracked discharge electrode material (inset: SEM image of analyzed sample).

3.6. Pitting Corrosion

Pitting corrosion is a local, accelerated dissolution of metal, which occurs as a result of the degradation of a protective passive layer on the metal surface [17]. This type of corrosion occurs only in specific areas in the form of spots or pits, often penetrating deep into the material. Pitting corrosion involves the formation of local pits due to the initiation of an anodic reaction by activating ions and a cathodic reaction in the presence of oxidizing agents. The bottom of the pit acts as the anode, and the metal dissolution takes place there. The walls surrounding the pit function as the cathode, and the oxygen reduction occurs [26].

Pits are a result of the reaction of metal with a corrosive agent on the metal surface. Figure 10 shows cylindrical losses of the material, which are examples of pits. In acid corrosion, iron in a dilute solution of hydrochloric or sulfuric acid undergoes a series of reactions [26]:

$$(\mathrm{Fe})_{metal} + (2\mathrm{HCl})_{liquid} \longrightarrow (\mathrm{FeCl_2}) + (\mathrm{H_2})_{gas}$$

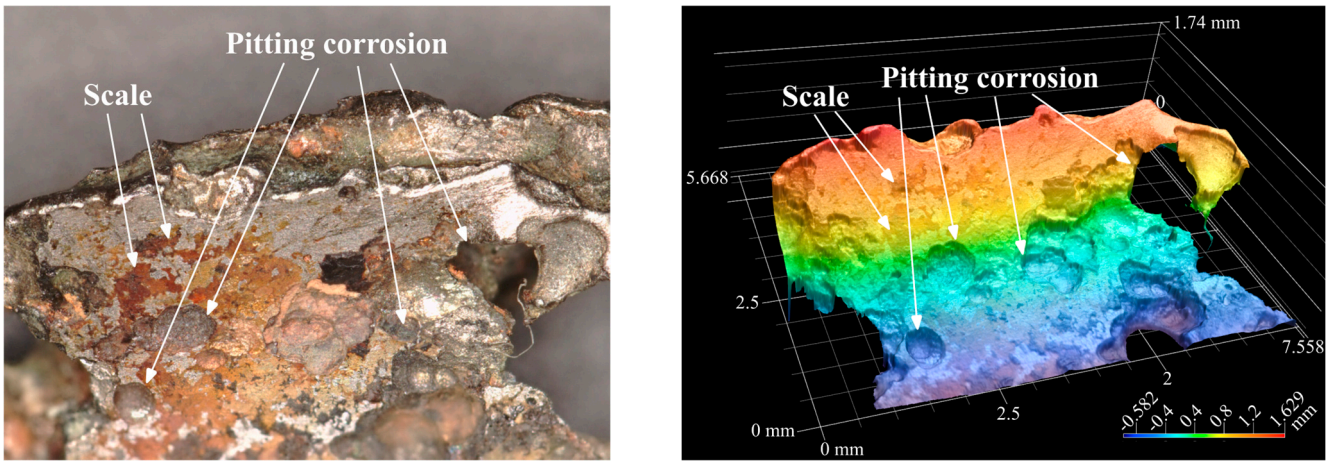
or

$$(\mathrm{Fe})_{metal} + (\mathrm{SO_4})_{liquid} \longrightarrow (\mathrm{FeSO_4}) + (\mathrm{H_2})_{gas}$$

where the subscripts *metal*, *liquid*, and *gas* indicate the following phases: solid metal, liquid aqueous solution, and gaseous, respectively. The amount of material loss in pits is a function of the time of exposure to the corrosive agent. In the presence of oxygen and moisture, a sequence of interdependent reactions of iron oxidation to Fe^{3+} and rust formation occur.

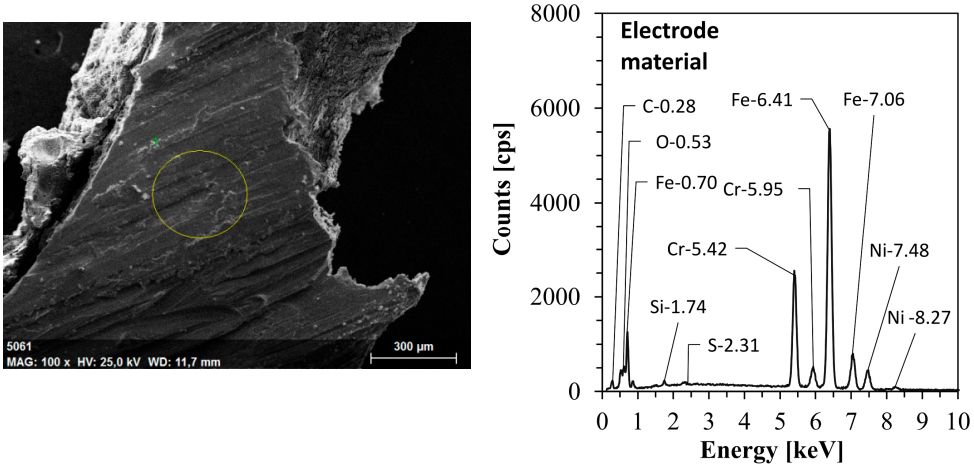
The corrosion of materials depends on the type of electric conductivity at the material–environment interface, and on the type of environment [27]. Pitting corrosion is a local form of corrosion, which occurs on passivated surfaces. The starting point of destruction may be the inclusions or grain boundaries on the surface. The aggressive anions penetrate through such places in the metal and create small cavities. The surface adjacent to the pitting corrosion places remains intact. The rate of pitting corrosion can be high due to the change in local chemical composition inside the pits [28].

The selected pit was mechanically cut in a direction perpendicular to the plane of the pit, and the elemental composition of three distinguished areas was examined in Figure 11.

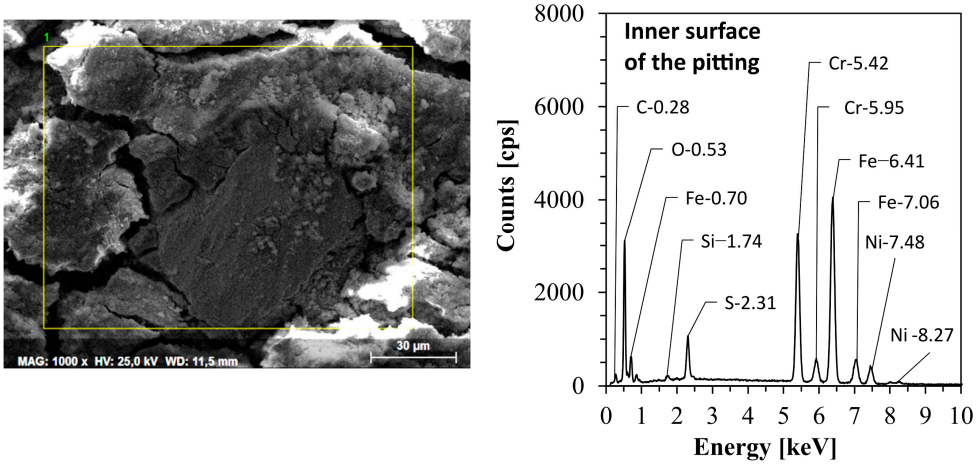


(**a**) (**b**)

Figure 10. (**a**) Image of various forms of pitting on the surface of a degraded metal electrode; (**b**) 3D profile (photos taken under a 3D profilometer Keyence VR-6200; courtesy of Keyence (Japan)).



(**a**)



(**b**)

Figure 11. SEM micrographs of cross-section of ESP discharge electrode (**left**) and EDS spectrum of selected places (**right**): (**a**) electrode fragment, cross-section of ESP discharge electrode (measurement area marked with circle 1); (**b**) close-up view of inner surface of pitting (scanning area marked with rectangle), inner surface of pitting in ESP discharge electrode.

Figure 11 shows a SEM micrograph of a cross-section of the ESP discharge electrode with a pitting. The elemental composition of the electrode was examined using the EDS method in the following areas: the original material (Figure 11a) and the inner surface of the pitting (Figure 11b). In comparing the elemental compositions of these different areas, it can be noticed that in the pit area, the content of basic metal components (iron, chromium, nickel) decreases, while the content of sulfur and oxygen increases. The results are confirmed by XRD measurements of the collected scale (cf. Section 3.7). As a result of corrosion, metal oxides (Fe_2O_3, CrO_2) or metal sulfides (FeS, Ni_3S_2, Cr_5S_8) are formed.

Papavinasam [29] reported that the pitting process consists of four stages: the formation of a surface layer on the metal surface, the initiation of pitting in localized areas of the metal surface, and the gradual propagation of pits, followed by a final deep penetration into the metal. Moreover, the metal corrosion rate is quite high at the stage of the activation reaction, as well as the rupture of the passivation layer. The corrosion activity is high, leading to the formation of spatially open pits (open pitting).

Figure 12 illustrates the development and propagation of cracks, resulting from the injection of fly ash particles into the fissures of an existing crack. Wear by spalling entails the dislodging of material particles from the substrate (Figure 12). This is caused by the propagation of micro-cracks initiated within the surface layer by micro-particles of ash-bonded friction elements.

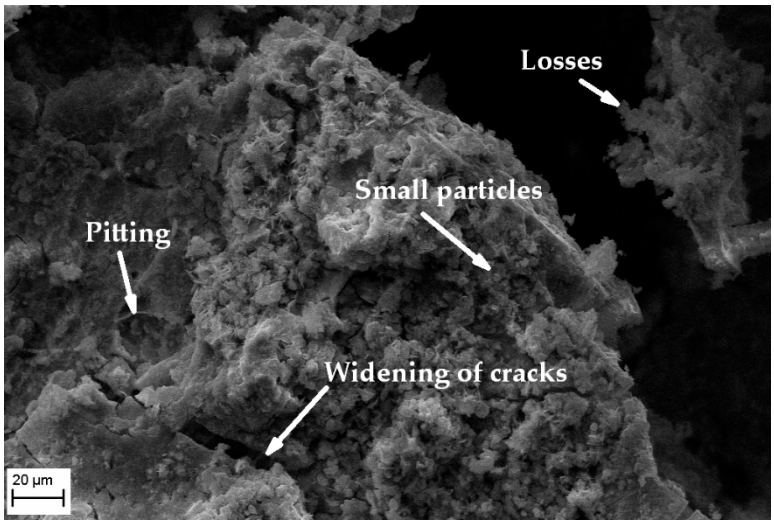
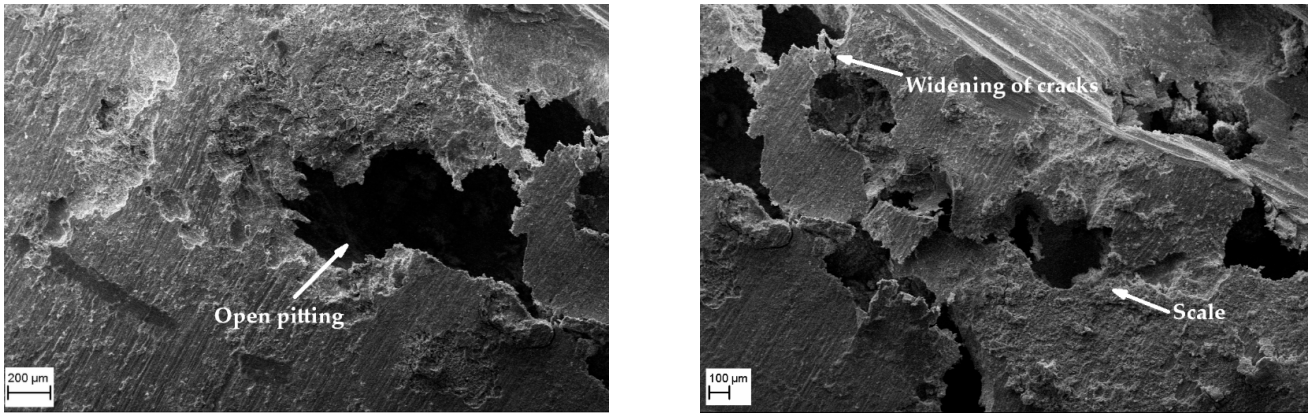


Figure 12. Fragment of discharge electrode (blade) with solid particles and damages (fissures and pitting) and peeling with detached element.

The formation of cracks (cf. Figures 7 and 8) initiates the deep degradation of the electrode material. Microscopic observations of the surface of electrode material revealed that the acid gasses had penetrated the cracks, causing the degradation of the electrode and the separation of small metal fragments (Figure 12).

The microstresses and structural heterogeneity of the material disrupt the cracking process to a varying degree. The corrosion cracks develop both along the grain boundaries (in the case of lower stresses) and intracrystalline [30]. Even in the case of plastic materials, fractures exhibit the characteristics of brittle fracture. Ultimately, the corrosive environment leads to the formation of open pits, as illustrated in Figure 13.



(**a**) (**b**)

Figure 13. SEM micrographs of open pits as a result of the degradation of electrode material due to corrosion processes (**a**), and scale at the edge of the pits (**b**).

The elemental composition (Figure 14) of the tested blade electrode indicates that there is not only fly ash on its surface, but also metal oxides originating from the electrode material. Scale elements, and the corrosion products, make it possible to determine the history of the corrosion process, and could be helpful in the development of effective corrosion prevention strategies. A key part of such an approach is the rapid identification of the corrosion products at the site of the scale.

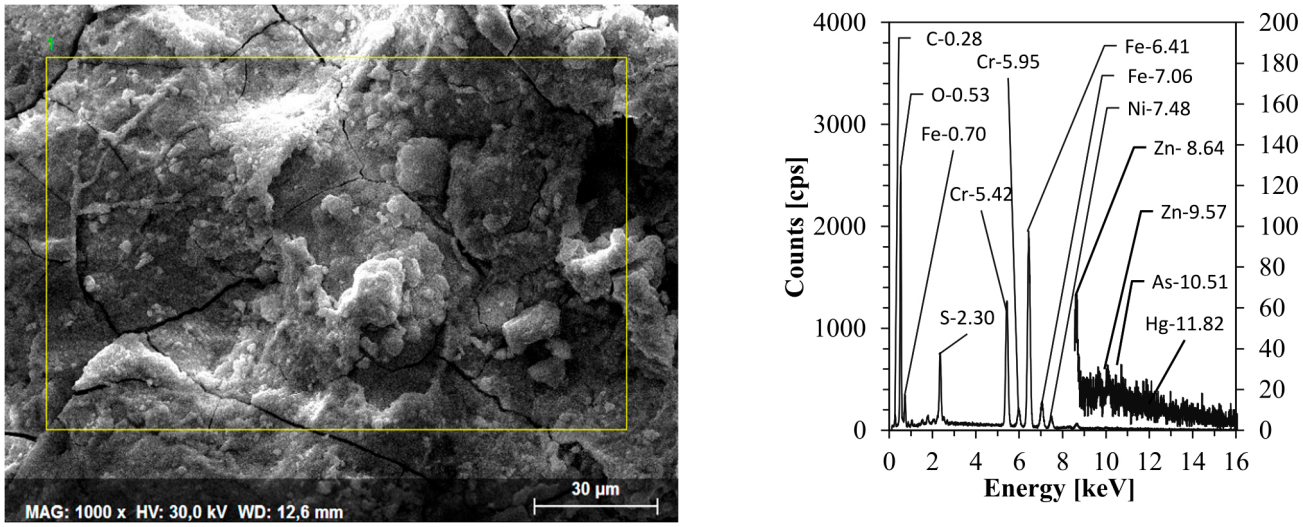


Figure 14. Scale mixed with the dust on the metal surface as a product of corrosion (**left**), and EDS spectrum of the scale on the surface of the discharge electrode (**right**).

Table 1 lists the elemental compositions of selected electrostatic precipitator discharge electrode locations: the cross-section of the construction metal of the ESP discharge electrode (Figure 11a) and various locations on the surface of the ESP discharge electrode (Figure 12).

3.7. Scale Crystallographic Analysis

When a metal material is exposed to a harsh environment, with oxidizing properties at elevated temperatures, a series of chemical reactions occur, resulting in the formation of reaction products. Depending on the conditions and composition of the material, these products may be volatile, liquid, or solid. These products are formed primarily on the surface of the material as a scale, but in some cases, the oxidation process may occur simultaneously or even exclusively in the depths of the metal material, as a result of the

diffusion of the oxidant into the material (internal oxidation), or, in the presence of sulfur oxide in the exhaust gas, it reacts with the electrode material to form sulfides or disulfides. During incomplete combustion (with oxygen deficiency), sulfides are formed in the scale. Conversely, when the combustion occurs with an excess of oxygen, metal oxides are formed. The alloy component will form a scale as a result of selective oxidation (e.g., Fe_2O_3, CrO_2). Figure 15 shows the XRD diffractogram of the scale deposit on the ESP discharge electrode. The presence of iron and chromium oxides, as well as iron, chromium, and nickel sulfides, was confirmed through X-ray diffraction (XRD) analysis.

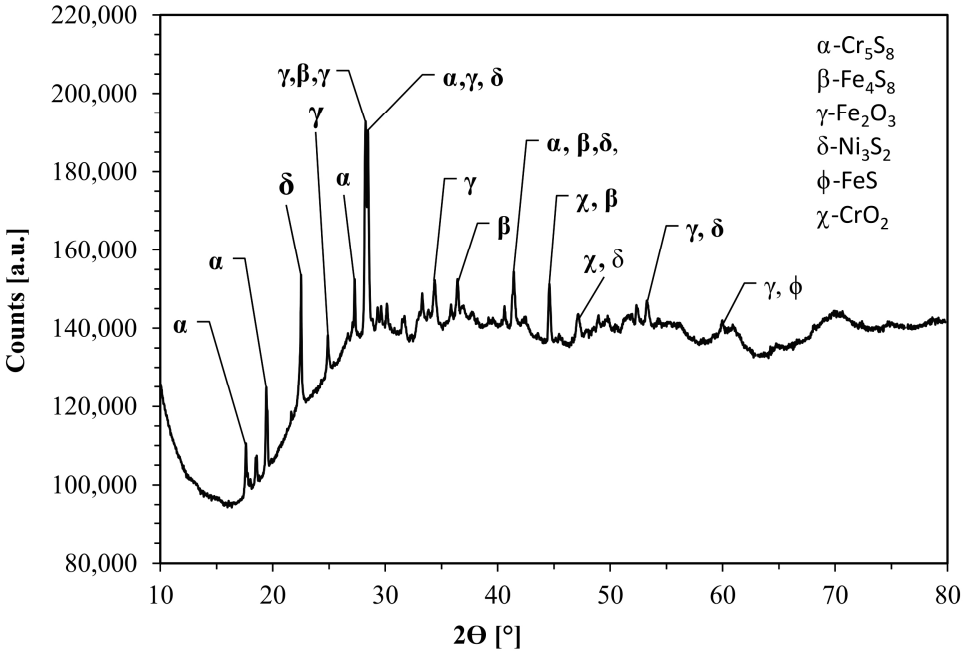


Figure 15. XRD diffractogram of scale and deposit of blade electrode.

4. Discussion

The investigation of discharge electrode degradation in an electrostatic precipitator was carried out. Given the lack of knowledge regarding the chemical composition and PM content of the exhaust gasses from an industrial waste incinerator, which can vary significantly, the physical and chemical causes of electrode degradation can be reconstructed ex-post and deduced from the traces of elements remaining at the electrode material only, or via a comparison of the effects of similar phenomena observed in laboratory experiments.

In the literature, only the problems of corrosion affecting boilers and heat exchangers, or exhaust pipes, are usually discussed. In these cases, the discussed processes involve high-temperature corrosion (from the boiler side) [31,32] or low-temperature corrosion (from the gas outlet side) [33,34]. In coal-fired boilers, the gas composition may vary slightly, but in the case of waste incineration plants, the flue gas composition may change depending on the type of waste being burned.

In the case of industrial waste incineration plants, the fuel components may include oil sludge, electronic parts, rubber, soil contaminated with pesticides, etc. Given the diverse nature of these components, it is challenging to ascertain the precise mechanisms, through which the electrostatic precipitator corrosion processes may occur.

There is an ongoing discussion in the literature regarding the possible mechanisms of corrosion and the influence of individual components in the flue gas on this process [31]. A review of the literature reveals the absence of information about the course of corrosion in exhaust gas treatment systems, where the temperature should be above the acid dew point.

In a solid waste incinerator, in which municipal wastes are used as a fuel, the corrosion of steel by chlorine and chlorides plays the main role. The corrosion process due to

the reaction of chlorides with oxides from the protective layer of the electrodes occurs as follows:

$$2NaCl + Fe_2O_3 + \frac{1}{2}O_2 \longrightarrow NaFe_2O_4 + Cl_2$$

$$4NaCl + Cr_2O_3 + \frac{5}{2}O_2 \longrightarrow 2Na_2CrO_4 + 2Cl_2$$

And the effect of chlorine (formed through the oxidation of HCl) [35] occurs as follows:

$$Fe + Cl_2 \longrightarrow FeCl_2$$

Due to relatively high vapor pressure at high gas temperatures, a continuous evaporation of $FeCl_2$ takes place, and metal chlorides diffuse outward from the scales. At the temperature of the flue gas in the electrostatic precipitator, this reaction could be negligible. The $FeCl_2$ reacts with O_2, resulting in Fe_2O_3 formation with Cl_2 gas emission:

$$4FeCl_2 + 3O_2 \longrightarrow 4Cl_2 + 2Fe_2O_3$$

For this reason, chlorine has not been detected in the corrosion layer with the EDS method.

In another way, the corrosion caused by SO_2 occurs at low temperatures of exhaust gasses. EDS and RDX analyses indicated that the sulfur phases occur on the discharge electrodes. General sulfur corrosion reactions could occur, forming metal salts [26].

Most corrosion processes involving water and aqueous solutions, called electrochemical corrosion, which might occur after water or acid condensation onto the electrodes, can be explained by the formation of corrosion microcells onto the surface. Local damage can lead to the perforation of the metal parts [36].

If a metal material is exposed to an environment with oxidizing properties at elevated temperatures, the reaction products are formed and form solid products called scales (cf. Figure 12), mainly on the surface of the material. The scale formed on the surface of the metal phase is dense, i.e., free from discontinuities and demonstrating sufficient adhesion to the substrate, thereby preventing the periodic detachment of the scale from the metal surface.

Corrosion is one of the inevitable problems of structural steel exposed to long-term exposure to waste gasses from the incineration of industrial waste. Corrosion is characterized by a uniform loss of the material of the surface layer.

Corrosion cracking can only occur when a corrosive environment combines with stresses and tensile forces (stress corrosion) [17]. In Figure 8, an area of a crack with a white circle is indicated. This crack is probably a result of stresses inside the material. Corrosion cracks can occur both along grain boundaries (in the case of lower stresses) and within the material's components (intracrystalline). Several typical stress corrosion cracks in the investigated electrode material are shown in Figure 12. The adsorption of sulfur compounds may occur in these cracks, resulting in their systematic widening (Figure 9).

Crack initiation occurs in brittle surface layers and is followed by a gradual expansion of these cracks into the inner zone of the metal. The cracking process is influenced by microstresses, which may result from temperature gradient or structural heterogeneity of the material. Often, in non-austenitic chromium–nickel steel material, the stress corrosion cracking results in the formation of groups of adjacent cracks. At the beginning of crack development, some dislocations and microdeformations can emerge at the surface (cf. Figure 8). The primary factor for crack development is the accelerated penetration of the corrosion environment into the crack crevices. Stress corrosion cracking can occur under the simultaneous action of a corrosive environment and tensile stresses. The microstresses and structural heterogeneity of the material distort the course of cracking.

The development of pitting corrosion occurs by increasing the pitting formed in the nucleation process and creating new corrosion zones. In the process of pitting corrosion, three

stages can be distinguished: the nucleation of pits on the metal surface, the development of pits, and finally, the perforation element (open pits).

The shape and size of the pits as well as volume of removed material change depending on the corrosive conditions. The quantity of material lost at the pitting site is a function of the acidic components and the moisture content [37]. The author of [37] reviewed the critical factors, which influence the pitting corrosion. The factors discussed include temperature, pressure, and surface roughness. The result of the corrosive environment is the formation of open pits, as illustrated in Figure 13. This mechanism suggests that the areas completely devoid of metal in this electrode are caused by acid gasses produced by waste incineration. The removed material accumulates at the edges of the pit in the form of scale or is removed with the flowing gas in the electrostatic precipitator.

Two- or multi-layer scales are formed on the surfaces of metals and alloys, where at least one of the layers, usually the innermost, is compact. The scales formed may be either single-phase or multi-phase, and they are compact throughout their cross-section, closely adhering to the substrate [36]. The scale is filled with fly ash particles, which absorbed Hg, As, and Cu compounds, as suggested by EDS measurement (Figure 14). A XRD diffractogram of the phase composition of scales on the electrode is shown in Figure 15.

Figure 16 shows that either sulfides or oxides are formed as an effect of corrosion, and these compounds are the most abundant in the scales.

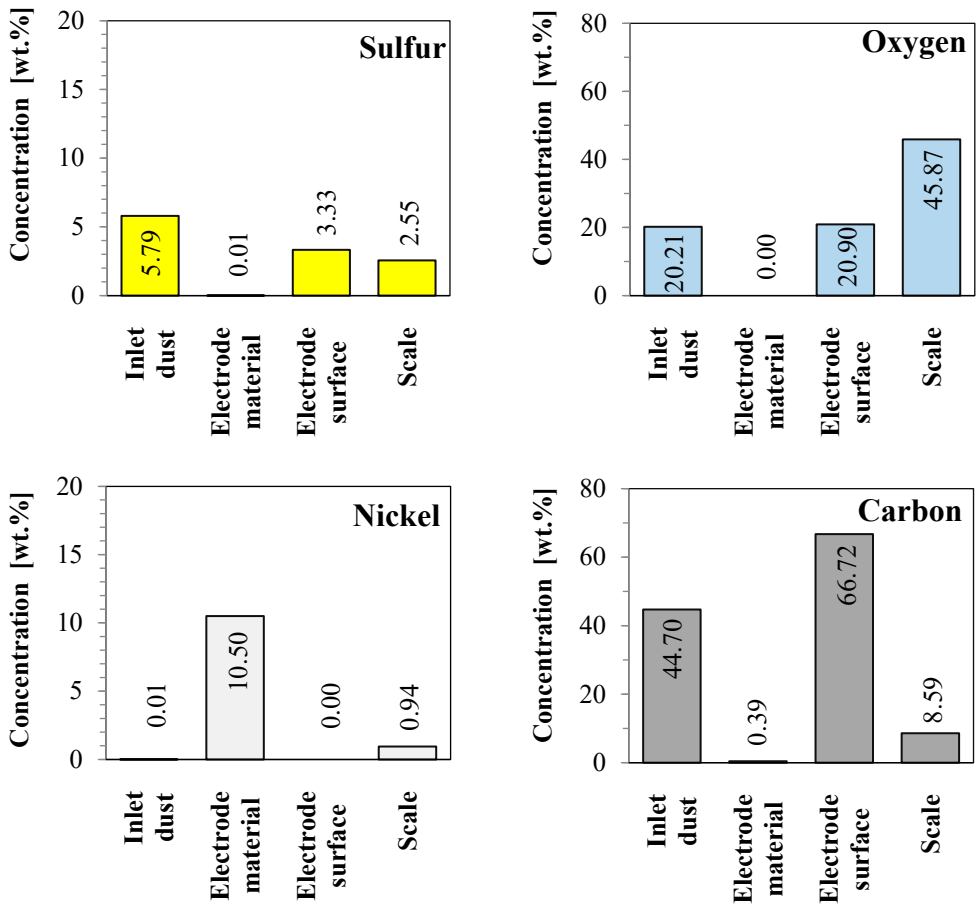


Figure 16. *Cont.*

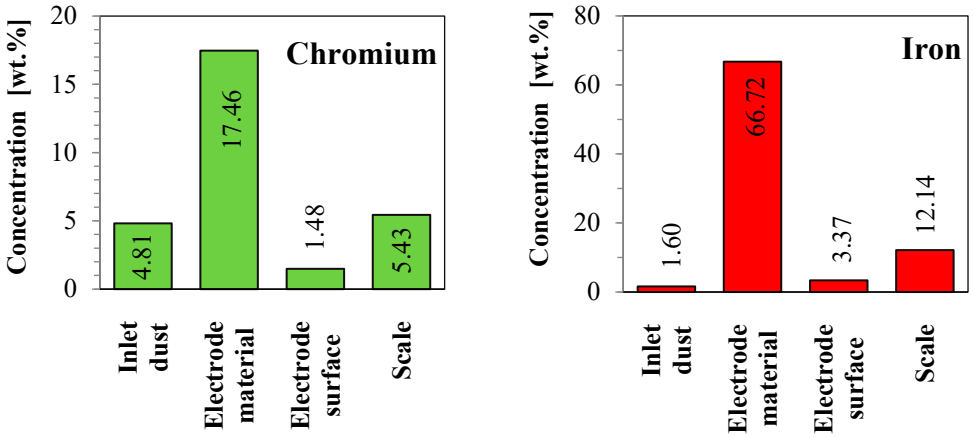


Figure 16. Variations in sulfur, iron, chromium, nickel, carbon, and oxygen content for the inlet dust and different electrode areas: ESP-deposited particulate fly ash on the discharge electrode, clean metal electrode surface, and degraded electrode material (scale) determined from the EDS spectrum.

Scale formation is also a common phenomenon observed in exhaust gasses. As a result of fly ash deposition on the discharge electrode, the sulfur reacts with the electrode material via "migrating" to the structure of the material. Figure 16 illustrates changes in the concentration of sulfur, phosphorus, iron, and chromium in different areas of the discharge electrode: in the fly ash deposited on the discharge electrode, clean metal electrode surface, degraded electrode material, and the scale. From this diagram, it is possible to estimate the migration of sulfur and phosphorus compounds (from exhaust gasses to scale) during the operation of the electrostatic precipitator. The sulfur compounds present in exhaust gasses penetrate both the created gaps in the electrode material, and are the main components of the scale.

The electric discharge plasma column that forms between the electrodes is a phenomenon that frequently occurs in electrostatic precipitators during back-corona discharge. This phenomenon can also cause material evaporation at a spot, resulting in the formation of small pits on the surface. The plasma column can be concentrated at a very small hot spot on the cathode, which causes the sputtering of the cathode material into the plasma region due to positive ion bombardment. Such an effect has been observed in many laboratory experiments. Another phenomenon occurs at the sharp edges of the discharge electrode, where the current density is particularly high, even at relatively small discharge currents, which was observed in other experiments [23,24]. The spot formed due to ion bombardment is difficult to distinguish from that due to electrochemical processes. In fact, both phenomena may occur simultaneously during an electrostatic precipitator operation.

5. Conclusions

This paper presents an analysis of the degradation of a discharge electrode operating in an electrostatic precipitator downstream of an industrial solid waste incinerator in Gdańsk (Poland). Several hypotheses on the potential sources of electrode degradation in incinerator plants, using incomplete data regarding the kind of combusted wastes, have been provided. The varying chemical composition of the waste materials results in vast changes in exhausts, both for the gaseous compounds and fly ash particles. The three main, most probable mechanisms of electrode degradation have been discussed: mechanical stresses due, for example, to temperature variation, corrosion caused by acid gasses in the exhausts, and electrical discharges due to back-corona discharge onset as in the case of fly ash of high resistivity. It is plausible that all of these mechanisms could operate simultaneously, and distinguishing between them is a separate task.

It was noticed in these investigations that industrial wastes have the potential to form large quantities of deposits on various parts of the electrostatic precipitator, particularly on the discharge electrodes. It was found through this research that almost all contaminants

emitted from the incinerator can leave their traces on the discharge electrodes. The most pronounced effects are those of sulfur and chlorine emissions in the form of acids, which cause electrode corrosion. A relatively large amount of sulfur compounds was found in the scale formed on the electrode's surface and within the metal crystalline structure. The deposits collected directly from the corroded discharge electrode have also structures consisting of a thin layer of oxides of iron, chromium, and nickel.

The elemental analysis and SEM investigation of the morphology of the electrode surface confirmed that several physical and chemical processes occur leading to the premature degradation of discharge electrodes. The degraded electrode generates lower discharge current, and thus the collection efficiency of electrostatic precipitator is decreased.

Another factor causing electrode degradation may also be fly ash gradually grinding its surface after collision. Contrary to exhausts from coal fired boilers, the morphology of particles from incinerators, their physical properties and chemical composition are also not well characterized and can vary significantly depending on the incinerator batch. Some investigations under SEM have demonstrated that the fly ash particles from municipal solid waste incinerators are irregular, porous aggregates with sharp edges [38–40], facilitating the electrode grinding, even when the gas velocity is relatively low.

The electrical breakdown streamers and pulseless glow or back-corona discharge can cause deformation, cracking, and permanent loss of discharge electrode material during ESP operation, and consequently degradation and loss of electrode mass. The presence of craters in the material initiates corrosion processes, enabling the penetration of sulfur compounds deeper into the metal.

Author Contributions: Conceptualization, T.C. and A.K.; methodology, T.C. and A.J.; investigation, A.K., A.M. and M.G.; data curation, A.T.S.; writing—original draft preparation, T.C.; writing—review and editing, A.J., A.M. and A.K.; visualization, A.T.S.; supervision, A.J. and AK. All authors have read and agreed to the published version of the manuscript.

Funding: This research was funded internally by the Institute of Fluid Flow Machinery, Polish Academy of Sciences, within the project No. O1/Z4/T3.

Institutional Review Board Statement: Not applicable.

Informed Consent Statement: Not applicable.

Data Availability Statement: Data available upon request.

Acknowledgments: We would like to thank KEYENCE INTERNATIONAL (Belgium) NV/SA for the preparation of optical microscopy photos and 3D optical profilometer images by D. Stańczyk and W. Eysymontt.

Conflicts of Interest: The authors declare no conflicts of interest.

References

1. Malcher, T. Erosion in ducts supplying exhaust gas to electrostatic precipitators due to gas-solid two-phase flow—Numerical simulation. *Inżynieria i Aparatura Chemiczna* **2012**, *51*, 354–355.
2. Chang, J.-S.; Kelly, A.; Crowley, J.M. *Handbook of Electrostatics Processes*; Marcel Dekker: New York, NY, USA, 1995.
3. Hoornweg, D.; Bhada-Tata, P. *What a Waste, Global Review of Solid Waste Management*; Urban Development & Local Government Unit, The World Bank: Washington, DC, USA, 2012.
4. Kaza, S.; Yao, L.; Bhada-Tata, P.; Van Woerden, F. *What a Waste 2.0: A Global Snapshot of Solid Waste Management to 2050*; Urban Development, The World Bank: Washington, DC, USA, 2018.
5. Van Caneghem, J.; Vandecasteele, C. Characterization of polycyclic hydrocarbons in flue gas and residues of a full scale fluidized bed combusting non-hazardous industrial waste. *Waste Manag.* **2014**, *34*, 2407–2413. [CrossRef]
6. Ribbing, C. Environmentally friendly use of non-coal ashes in Sweden. *Waste Manag.* **2007**, *27*, 1428–1435. [CrossRef] [PubMed]
7. Diabaté, S.; Bergfeldt, B.; Plaumann, D.; Übel, C.; Weiss, C. Anti-oxidative and inflammatory responses induced by fly ash particles and carbon black in lung epithelial cells. *Anal Bioanal. Chem.* **2011**, *401*, 3197–3212. [CrossRef] [PubMed]
8. Delfino, R.J.; Sioutas, C.; Malik, S. Potential Role of Ultrafine Particles in Associations between Airborne Particle Mass and Cardiovascular Health. *Environ. Health Perspect.* **2005**, *113*, 934–946. [CrossRef] [PubMed]
9. Li, M.; Wang, C.; Cen, K.; Ni, M.; Li, X. PCDD/F emissions during startup and shutdown of a hazardous waste incinerator. *Chemosphere* **2017**, *181*, 645–654. [CrossRef]

10. Chou, J.-D.; Wey, M.-Y.; Chang, S.-H. Evaluation of the distribution of Pb, Cu, and Cd from MSWI fly ash treatment by sequential extraction procedure. *J. Hazard. Mater.* **2009**, *162*, 1000–1006. [CrossRef]
11. Le Forestier, L.; Libourel, G. Characterization of Flue Gas Residues from Industrial Solid Waste Combustors. *Environ. Sci. Technol.* **1998**, *32*, 2250–2256. [CrossRef]
12. Commission Implementing Decision (EU) 2019/2010 of 12 November 2019 Establishing the Best Available Techniques (BAT) Conclusions, under Directive 2010/75/EU of the European Parliament and of the Council, for Waste Incineration (Notified under Document C (2019) 7987). Available online: https://eur-lex.europa.eu/legal-content/EN/TXT/PDF/?uri=CELEX:32019D2010 (accessed on 3 July 2024).
13. Aurell, J.; Barnes, M.; Gullett, B.K.; Holder, A.; Eninger, R. Methodology for characterizing emissions from small (0.5–2 MTD) batch-fed gasification systems using multiple waste composition. *Waste Manag.* **2019**, *87*, 398–406. [CrossRef]
14. Machnik, R.; Nocuń, M. Effect of anti-corrosion coatings of corona electrodes on selected operating parameters of industrial electrostatic precipitators. *Eksploat. i Niezawodn. Maint. Reliab.* **2014**, *16*, 56–60.
15. Ali, M.; Alam, K.; Al-Majali, Y.T.A.; Kennedy, M. Novel hybrid composite discharge electrode for electrostatic precipitator. *J. Air Waste Manag. Assoc.* **2017**, *67*, 1036–1045. [CrossRef] [PubMed]
16. Kim, H.-J.; Kim, M.; Han, B.; Woo, C.G.; Zouaghi, A.; Zouzou, N.; Kim, Y.-J. Fine particle removal by a two-stage electrostatic precipitator with multiple ion-injection-type prechargers. *J. Aerosol Sci.* **2019**, *130*, 61–75. [CrossRef]
17. Hall, H.J.; Katz, J. Corrosion problems and solutions for electrostatic precipitators. *J. Air Pollut. Control Assoc.* **1976**, *26*, 312–317. [CrossRef]
18. Finnie, I. Erosion of surfaces by solid particles. *Wear* **1960**, *3*, 87–103. [CrossRef]
19. Czech, T.; Sobczyk, A.T.; Jaworek, A. Optical emission spectroscopy of point-plane corona and back-corona discharges in air. *Eur. Phys. J. D* **2011**, *65*, 459–474. [CrossRef]
20. Czech, T.; Sobczyk, A.T.; Jaworek, A.; Krupa, A. Corona and back discharges in flue-gas simulating mixture. *J. Electrostat.* **2012**, *70*, 269–284. [CrossRef]
21. Jaworek, A.; Czech, T.; Rajch, E.; Lackowski, M. Laboratory studies of back-discharge in fly ash. *J. Electrostat.* **2006**, *64*, 326–337. [CrossRef]
22. de Cadiz, M.C.; Arrabal, A.L.; Lantada, A.D.; Aguirre, M.V. Materials degradation in non-thermal plasma generators by corona discharge. *Sci. Rep.* **2021**, *11*, 24175. [CrossRef]
23. Czech, T.; Sobczyk, A.T.; Jaworek, A.; Krupa, A.; Rajch, E. Studies of corona and back discharges in carbon dioxide. *Eur. Phys. J. D* **2013**, *67*, 23. [CrossRef]
24. Czech, T.; Sobczyk, A.T.; Jaworek, A. Light emission spectra of molecules in negative and positive back discharges in nitrogen with carbon dioxide mixture at atmospheric pressure. *Eur. Phys. J. D* **2015**, *69*, 223. [CrossRef]
25. Alterary, S.S.; Marei, N.H. Fly ash properties, characterization, and applications: A review. *J. King Saud Univ. Sci.* **2021**, *33*, 101536. [CrossRef]
26. Kaesche, H. *Corrosion of Metals: Physicochemical Principles and Current Problems*; Springer: Berlin/Heidelberg, Germany, 2003; ISBN 13 978-3-642-05620-8.
27. Ito, M. Time-dependent power laws in the oxidation and corrosion of metals and alloys. *Sci. Rep.* **2022**, *12*, 6944. [CrossRef] [PubMed]
28. Alvarez, M.G.; Galvele, J.R. 2.04—Pitting corrosion. In *Shreir's Corrosion*, 1st ed.; Cottis, R., Graham, M., Lindsay, R., Lyon, S., Richardson, J., Scantlebury, J., Stott, F., Eds.; Elsevier: Amsterdam, The Netherlands, 2010; Volume 1, pp. 772–800, ISBN 978-0-444-52787-5.
29. Papavinasam, S. Pitting corrosion. In *Trends in Oil and Gas Corrosion Research and Technologies*, 1st ed.; El-Sherik, A.M., Ed.; Woodhead Publishing: Cambridge, NY, USA, 2017; pp. 663–688.
30. Cheng, F. *Fundamentals of Stress Corrosion Cracking in Book Stress Corrosion Cracking of Pipelines*; John Wiley & Sons, Inc.: New York, NY, USA, 2013. [CrossRef]
31. Li, H.; Liu, H.; Huang, Y.; Chen, X.; Zhang, X.; Li, J.; Xu, L. Mechanism of coupling corrosion caused by flue gas and deposits in municipal solid waste incinerator: Roles of H_2O(g), HCl, and SO_2. *Corros. Sci.* **2024**, *231*, 111933. [CrossRef]
32. Zhang, X.; Liu, H.; Chen, T.; Li, H.; Huang, Z.; Yu, Y.; Yao, H. Mechanism of coupling corrosion caused by flue gas and deposits in municipal solid waste incinerator: Resistance of HVOF-NiCr coating. *Fuel* **2023**, *342*, 127845. [CrossRef]
33. Vainio, E.; Ruozzi, A.; Kinnunen, H.; Laurén, T.; Hupa, L. Low-temperature corrosion in a BFB boiler firing biomass and waste streams—Online measurement technique for monitoring deposit corrosivity. *Fuel* **2024**, *371*, 131864. [CrossRef]
34. Pan, P.; Zhou, W.; Chen, H.; Zhang, N. Investigation on the Corrosion of the Elbows in the Flue Gas Cooler of a 600 MW Coal-Fired Power Plant. *ACS Omega* **2020**, *5*, 32551–32563. [CrossRef]
35. Grabke, H.J.; Reese, E.; Spiegel, M. The effect of chlorides, hydrogen chloride and sulfur dioxide in the oxidation of steels below deposits. *Corros. Sci.* **1995**, *37*, 1023–1043. [CrossRef]
36. Burkett, D.A. Characterization of corrosion and scaling products with portable X-ray diffraction. In Proceedings of the 15th Asia Pacific Conference for Non-Destructive Testing (APCNDT2017), Singapore, 13–17 November 2017.
37. Obeyesekere, N.U. Pitting corrosion. In *Woodhead Publishing Series in Energy, Trends in Oil and Gas Corrosion Research and Technologies*; El-Sherik, A.M., Ed.; Woodhead Publishing: Cambridge, UK, 2017. [CrossRef]

38. Taylor, E.T.; Dykstra, E.J.; Krzanowski, J.E.; Domingo, D.S.; Staempfli, D.; Martin, J.R.; Erickson, P.M. Comprehensive approach toward understanding element speciation and leaching behavior in municipal solid waste incineration electrostatic precipitator ash. *Environ. Sci. Technol.* **1995**, *29*, 629–646. [CrossRef]
39. Li, M.; Xiang, J.; Hu, S.; Sun, L.-S.; Su, S.; Li, P.-S.; Sun, X.-X. Characterization of solid residues from municipal solid waste incinerator. *Fuel* **2004**, *83*, 1397–1405. [CrossRef]
40. Bayuseno, A.P.; Schmahl, W.W. Characterization of MSWI fly ash through mineralogy and water extraction. *Resour. Conserv. Recycl.* **2011**, *55*, 524–534. [CrossRef]

Disclaimer/Publisher's Note: The statements, opinions and data contained in all publications are solely those of the individual author(s) and contributor(s) and not of MDPI and/or the editor(s). MDPI and/or the editor(s) disclaim responsibility for any injury to people or property resulting from any ideas, methods, instructions or products referred to in the content.